Magnetic skyrmion-based synaptic devices

Magnetic skyrmions are promising candidates for next-generation information carriers, owing to their small size, topological stability, and ultralow depinning current density. A wide variety of skyrmionic device concepts and prototypes have recently been proposed, highlighting their potential applications[1]. Furthermore, the intrinsic properties of skyrmions enable new functionalities that may be inaccessible to conventional electronic devices. Here, we report on a skyrmion-based artificial synapse device for neuromorphic systems[2]. The synaptic weight of the proposed device can be strengthened/weakened by positive/negative stimuli, mimicking the potentiation/depression process of a biological synapse. Both short-term plasticity (STP) and long-term potentiation (LTP) functionalities have been demonstrated with micromagnetic simulations. This proposal suggests new possibilities for synaptic devices in neuromorphic systems with adaptive learning function.

The primary components of the proposed skyrmionic synaptic device are a ferromagnetic (FM) layer (e.g., Co) on a heavy metal (HM, e.g., Pt) and an energy barrier. The FM layer has perpendicular magnetic anisotropy (PMA), and the Dzyaloshinskii-Moriya Interaction (DMI) is generated at the interface between the FM layer and the HM, shown in Fig 1.

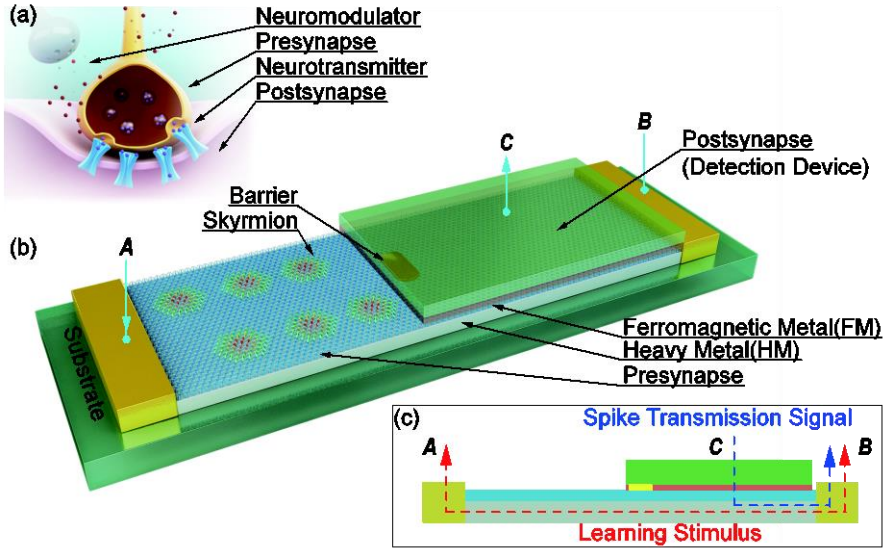

Fig 1. Schematic of (a) a biological synapse and (b) the proposed skyrmionic synaptic device. To mimic a neuromodulator, a bidirectional learning stimulus flowing through the HM from terminal

A to terminal B (or vice versa) drives skyrmions into (or out of) the postsynapse region to increase (or decrease) the synaptic weight, as shown in (c), mimicking the potentiation/depression process of a biological synapse.

The proposed skyrmionic synaptic device was numerically simulated by solving the Landau–Lifshitz–Gilbert (LLG) equation with spin transfer torques as follows[3]:

$$\frac{d\boldsymbol{m}}{dt} = -|\gamma|\boldsymbol{m} \times \boldsymbol{h}_{eff} + \alpha \boldsymbol{m} \times \frac{d\boldsymbol{m}}{dt} + \frac{u}{t}\boldsymbol{m} \times (\boldsymbol{m}_p \times \boldsymbol{m})$$

where $\boldsymbol{m} = \boldsymbol{M}/M_s$ is the reduced magnetization, $M_s = 580kA/m$ is the saturation magnetization, $\gamma = -2.211 \times 10^5 mA^{-1}s^{-1}$ is the gyromagnetic ratio, $\boldsymbol{h}_{eff} = \boldsymbol{H}_{eff}/M_s$ is the reduced effective field, $\alpha = 0.3$ is the Gilbert damping, t is the thickness of the ferromagnetic layer, $u = \gamma(\hbar jP/2eM_s)$, j is the density of the spin current, and P=0.4 is the spin polarization.

Three primary operation modes are developed for our proposed synaptic device: the initialization mode, the potentiation mode, and the depression mode. Before we illustrate the operation modes of the proposed synaptic device, we define two terms: (a) positive stimulus, which signifies an electric current with an amplitude of 5 MA/cm^2 flowing from terminal A to terminal B; and (b) negative stimulus, which signifies an electrical current with amplitude of 5 MA/cm^2 flowing from terminal B to terminal A. In the initialization mode (from 0 to 35 ns), skyrmions are generated in the presynapse region of the device. Owing to the repulsion between skyrmions and the nanotrack edges, a threshold value for the total number of skyrmions (11 skyrmions in our design, with a 120-nm-wide nanotrack) in the presynapse region of the device will be reached. This threshold value determines the programming resolution of the synaptic weight of the device. In the potentiation mode (from 35 to 65 ns; see Fig 2(b)), a positive stimulus drives skyrmions from the presynapse region into the postsynapse region, increasing the synaptic weight of the device. Similarly, in the depression mode (from 87 to 117 ns; see Fig 2(c)), a negative stimulus drives skyrmions from the postsynapse region into the presynapse region, decreasing the synaptic weight of the device. The red curve in Fig 2(d) shows the normalized mz (i.e., the average magnetization component in the z direction) of the postsynapse region of the device. The shifting of mz corresponds to the variation in the skyrmion number and size. It should be noted that two skyrmions fail to pass through the barrier in both the potentiation and depression modes. This can be explained as a

consequence of the insufficiency of the total driving force, which consists of the driving force of the electric current and the repulsion force of the skyrmions. Taking the potentiation mode as an example, as skyrmions move into the postsynapse region, the repulsion force of the skyrmions in the presynapse region, which favors skyrmion motion from the presynapse region into the postsynapse region, will decrease, whereas the repulsion force of the skyrmions in the postsynapse region, which hinders skyrmion motion from the presynapse region into the postsynapse region, will increase. Meanwhile, the driving force of the electric current (herein we consider a direct current, DC) and the repulsion force of the barrier remain unchanged. Finally, all these forces enter an equilibrium state, leaving two skyrmions in the presynapse region. The synaptic weight of the postsynapse region of the device can be determined by measuring the magnetoresistance through the detection device at terminal C. This dynamic weight behavior, illustrated in Fig 2(d), demonstrates the stimulus-induced synaptic plasticity of the proposed skyrmionic device. It is worth noting that the size of the skyrmions also depends on the driving force and the repulsion force, as shown in the snapshots in Fig 2. As soon as the stimulus is turned off, the compressed skyrmions begin to expand into an equilibrium state, leading to an obvious change of mz in the postsynapse region. To illustrate the potentiation/depression dynamics without considering the size impact of skyrmions, the change of the skyrmion number (Nsk) in the postsynapse region is also depicted as the blue line in Fig 2(d).

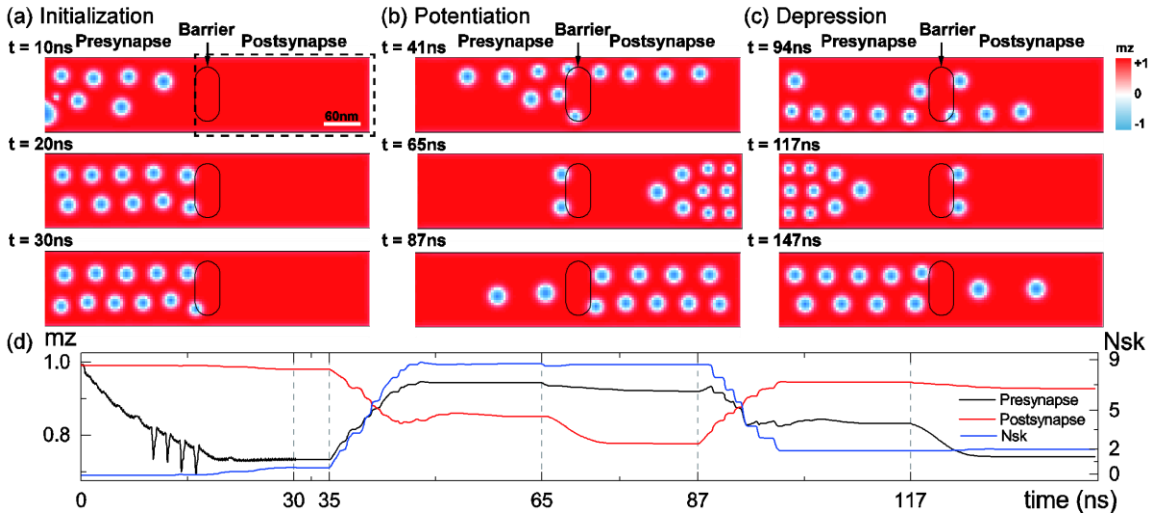

Fig 2. Micromagnetic simulations of the operation modes of our proposed skyrmionic synaptic device. (a) Initialization (from 0 to 35 ns): skyrmions are generated in the presynapse region; (b) potentiation mode (from 35 to 87 ns): a positive stimulus (from 35 to 65 ns) drives skrymions from the presynapse region to the postsynapse region, increasing the synaptic weight of the device; and (c) depression mode (from 87 to 147 ns): a negative stimulus (from 87 to 117 ns) drives skrymions from the postsynapse region into the presynapse region, decreasing the synaptic weight of the device. In each operation mode, the device is relaxed to the equilibrium state. (a), (b), and (c) show snapshots of the magnetization of the nanotrack, and (d) shows the time-resolved normalized mz (the average magnetization component in the z direction) of the presynapse and postsynapse regions. The skyrmion number Nsk of the postsynapse is also shown in (d).

We also investigated the dynamics of the synaptic plasticity of the proposed device with respect to the stimulus characteristics. In specific, we considered three stimulus configurations: case 1, 1.5 ns in duration at 5-ns intervals, as shown in Fig 3(b); case 2, 1 ns in duration at 2-ns intervals, as shown in Fig 3(c); and case 3, 1 ns in duration at 5-ns intervals, as shown in Fig 3(d).

Each configuration consists of eight stimulus pulses. We monitored the magnetoconductance change of the postsynapse region of the device, expressed by the ratio to the magnetoconductance without skyrmions (G0). As these figures show, cases 1 and 2 demonstrate an LTP property, while case 3 demonstrates an STP property. Compared with cases 1 and 3, with the same interval, a proper stimulus duration is required to transfer STP to LTP. Cases 2 and 3 demonstrate that the interval of the stimulus also plays an essential role in the device's plasticity. To eliminate the effect of conductance variation due to skyrmion size oscillation, the skyrmion number (Nsk) is also calculated, as shown in Fig 3(e), which corresponds to the above analyses.

The STP and LTP of the proposed synaptic device can be explained by the competition between the driving force provided by the electric current and the repulsion force provided by the barrier when the skyrmion passes through the barrier. When the skyrmion approaches the barrier, the repulsion force of the barrier increases, as shown in the energy profile of Fig 3(a). Upon receipt of an input stimulus, the driving force of the electric current proceeds the skyrmion uphill along the force energy profile (from point 1 to point 2). However, the skyrmion falls back to point 1, if the input stimulus is not of sufficient duration and frequency, corresponding to STP. Otherwise, if the stimulus is of sufficient duration and/or frequency, the skyrmion will not have enough time to reach point 1 and ultimately will be able to pass the barrier until to point 3, corresponding to

LTP. Once the skyrmion passes through the barrier, it is difficult to move back to the initial position. This behavior is consistent with the psychological model of a biological synapse.

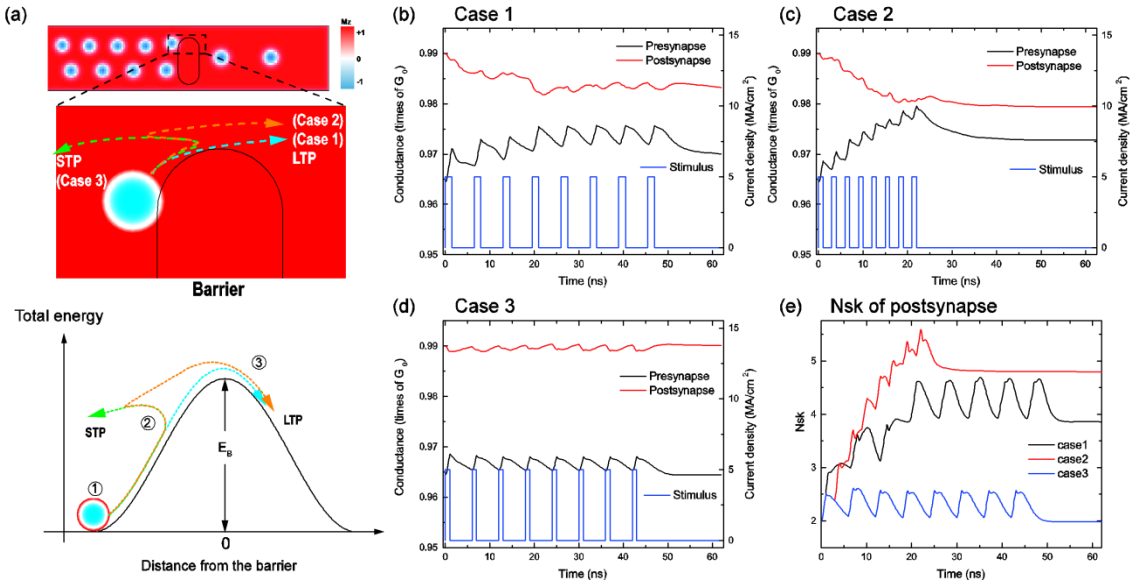

Fig 3. (a) Illustration of STP and LTP of the proposed synaptic device. (b), (c), and (d) Conductance variations of the postsynapse under different stimulus pulses: (b) case 1, 1.5 ns in duration with 5-ns interval; (c) case 2, 1 ns in duration with 2-ns interval; and (d) case 3, 1 ns in duration with 5-ns interval. (e) Comparison of the skyrmion number Nsk change rate among the three cases.

Weisheng Zhao, professor, school of electronics and information engineering, Beihang University, E-mail: weisheng.zhao@buaa.edu.cn

References

[1]Kang, W., Huang, Y., Zhang, X., Zhou, Y. & Zhao, W. Skyrmion-Electronics: An Overview and Outlook. Proc. IEEE 104, 2040–2061 (2016).

[2]Huang, Y., Kang, W., Zhang, X., Zhou, Y. & Zhao, W. Magnetic skyrmion-based synaptic devices. Nanotechnology 28, 08LT02 (2017).

[3]Sampaio, J., Cros, V., Rohart, S., Thiaville, A. & Fert, A. Nucleation, stability and current-induced motion of isolated magnetic skyrmions in nanostructures. Nat. Nanotechnol. 8, 839–44 (2013).